

Evolutionarily conserved coupling of adaptive and excitable networks mediates eukaryotic chemotaxis

Ming Tang, Mingjie Wang, Changji Shi, Pablo A. Iglesias, Peter N. Devreotes & Chuan-Hsiang Huang

Nature Communications 5, Article number: 5175 doi:10.1038/ncomms6175

Received 30 July 2014 Accepted 06 September 2014 Published 27 October 2014

Abstract

Numerous models explain how cells sense and migrate towards shallow chemoattractant gradients. Studies show that an excitable signal transduction network acts as a pacemaker that controls the cytoskeleton to drive motility. Here we show that this network is required to link stimuli to actin polymerization and chemotactic motility and we distinguish the various models of chemotaxis. First, signalling activity is suppressed towards the low side in a gradient or following removal of uniform chemoattractant. Second, signalling activities display a rapid shut off and a slower adaptation during which responsiveness to subsequent test stimuli decline. Simulations of various models indicate that these properties require coupled adaptive and excitable networks. Adaptation involves a G-protein-independent inhibitor, as stimulation of cells lacking G-protein function suppresses basal activities. The salient features of the coupled networks were observed for different chemoattractants in *Dictyostelium* and in human neutrophils, suggesting an evolutionarily conserved mechanism for eukaryotic chemotaxis.

Subject terms: Biological sciences Biophysics Cell biology Systems biology

Introduction

Chemotaxis, the directed migration of cells in response to extracellular chemical gradients, plays important roles in embryonic development and wiring of the nervous system, and in critical processes in adults such as immune response, wound healing, organ regeneration and stem cell homing. Derangements of chemotaxis underlie the pathogenesis of metastatic cancers and allergic, autoimmune and cardiovascular diseases. Although many behavioural features of chemotactic responses are shared among most motile eukaryotic cells, it is not clear to what extent the overall molecular paradigm is conserved.

Chemotaxis involves the integration of motility, polarity and gradient sensing^{1,2}. Cells move by extending protrusions stochastically. Typically, they have an axis of polarity with a relatively active front and more contractile rear. Eukaryotic cells are able to sense differences in chemoattractant—in some cells such as *Dictyostelium* amoeba and human neutrophils as little as 2%—across their length^{3,4,5,6}. These cells can sense gradients over a range of ambient concentrations, because they are able to adapt to the average level.

A series of conceptual models have been proposed to explain one or the other of these features of chemotaxis². Excitable networks (ENs) incorporating a variety of feedback schemes account for the stochastic behaviour during migration^{7,8,9,10}. Local excitation, global inhibition (LEGI) models explain the cells' ability to respond to changes in chemoattractant but adapt when the level is held constant^{11,12,13,14,15}. Frontness–backness models lead to symmetry breaking and polarity^{16,17,18,19}. Alone, however, none of these models satisfactorily explains the spectrum of observations displayed by chemotactic cells. For example, ENs cannot explain adaptation to constant stimuli and LEGIs lack the dynamic behaviour observed in chemotactic cells. Furthermore, none of these models can account for the multiple temporal phases displayed in the responses to chemotactic stimuli^{20,21,22,23,24,25}. A number of models have combined several of these features with promising results but have not been thoroughly tested^{26,27,28,29,30}.

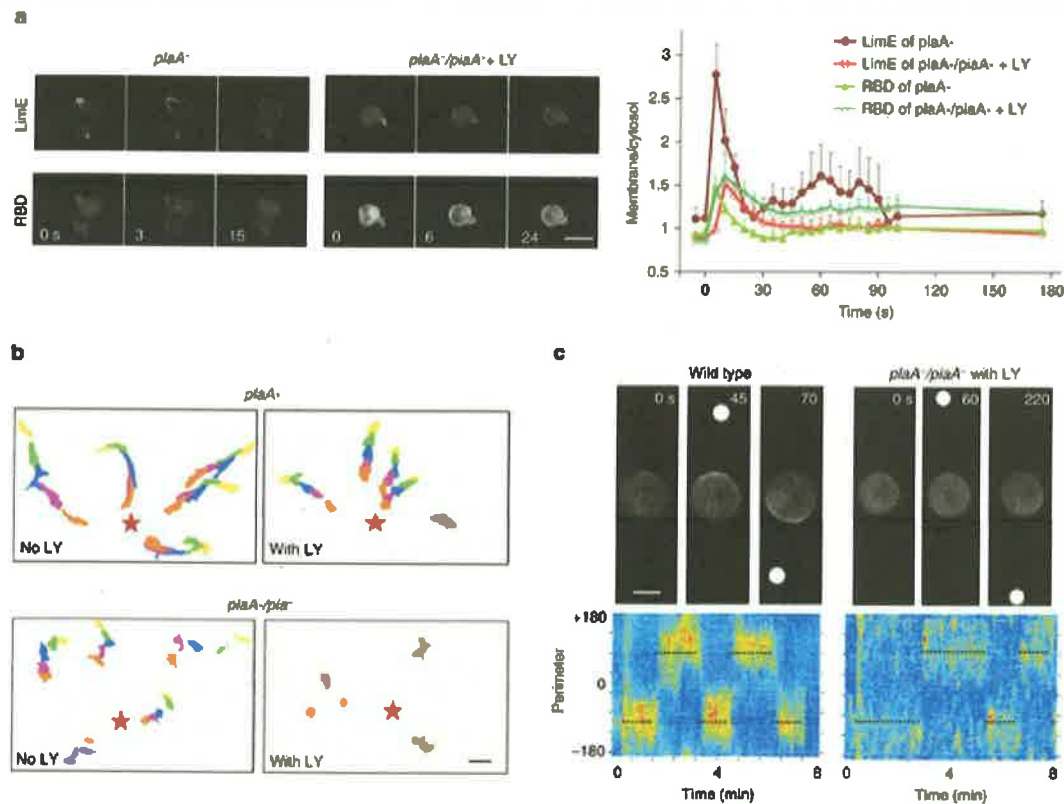
Recently, we demonstrated that cell motility requires independent but coupled signal transduction and cytoskeletal networks³¹. We found that the signal transduction network, comprising Ras small GTPases, phosphoinositide 3-kinases (PI3Ks) and Rac small GTPases, displays features of excitability and therefore designated it as STEN (signal transduction EN). Here, by eliminating multiple pathways simultaneously, we demonstrate that activation of STEN by chemoattractant is critical for chemotactic motility but not directional sensing. By examining the pattern of response to combinations of spatial and temporal stimuli with different chemoattractants, we show that STEN is controlled by an adaptive LEGI mechanism involving an incoherent feedforward topology, ruling out other proposed schemes. We show that the main features of this scheme can also explain the kinetics of activation and adaptation of human neutrophils to the chemoattractant *N*-formylmethionyl-leucyl-phenylalanine (fMLP). As the stochastic firing of STEN serves as a pacemaker to drive cytoskeletal activity and motility, our results provide the experimental evidence supporting a new paradigm for eukaryotic chemotaxis.

Results

Activation of the STEN is essential for directed migration

We previously reported that combined block of PI3K, *PLA2* and TorC2 pathways greatly reduced random migration, and as shown in Fig. 1a this combination of defects inhibits chemoattractant-elicited actin polymerization³¹. In cells lacking *PLA2*, TorC2 subunit *PiaA* and treated with the PI3K inhibitor *LY294002*, the initial peak of recruitment of actin-binding protein *LimE* to the membrane was reduced to 30% and the secondary peaks were absent (Fig. 1a). In biochemical assays, the initial peak of F-actin was reduced to 20% (Supplementary Fig. 1a). Importantly, chemoattractant-induced Ras activation rose rapidly to the same peak in *plaA*⁻ cells and cells lacking all three pathways. Consistent with Charest *et al.*³², whereas in *plaA*⁻ cells activity returned quickly to basal levels, in the cells lacking all three pathways, it declined more slowly and remained at about 20% of the peak value even 3 min after stimulation.

Figure 1: STEN is essential for directed migration.



(a) *LimE*-RFP and RBD-GFP were co-expressed in *plaA*⁻ or *plaA*⁻/*piaA*⁻ *Dictyostelium* cells treated with 50 μM LY. The cells were stimulated with 1 μM cAMP at 0 s. Left: representative images from time-lapse videos captured at 3 s per frame. Right: quantification of membrane to cytosol ratio of RBD and *LimE* (means ± s.d. of *n*=3 cells each) over time. Scale bar, 10 μm. (b) Chemotaxis of cells developed for 5 h treated with 50 μM LY or control volume of DMSO. Scale bar, 20 μm. Cell migration towards the tip of a micropipette

filled with 1 μM cAMP (red stars) was recorded at 30 s intervals. Five representative cells in each movie were outlined and traced every 5 frames. (c) Cells were treated with 5 μM latrunculin. A micropipette filled with 1 μM cAMP was placed next to the cell at 20 s and switched to the opposite side of the cell several times. Top: representative images showing the direction of RBD-GFP patches in cells. White dots indicate the location of the micropipette tip. Scale bar, 5 μm . Bottom: kymograph showing the activity of RBD-GFP. Dotted lines indicate direction of the gradient.

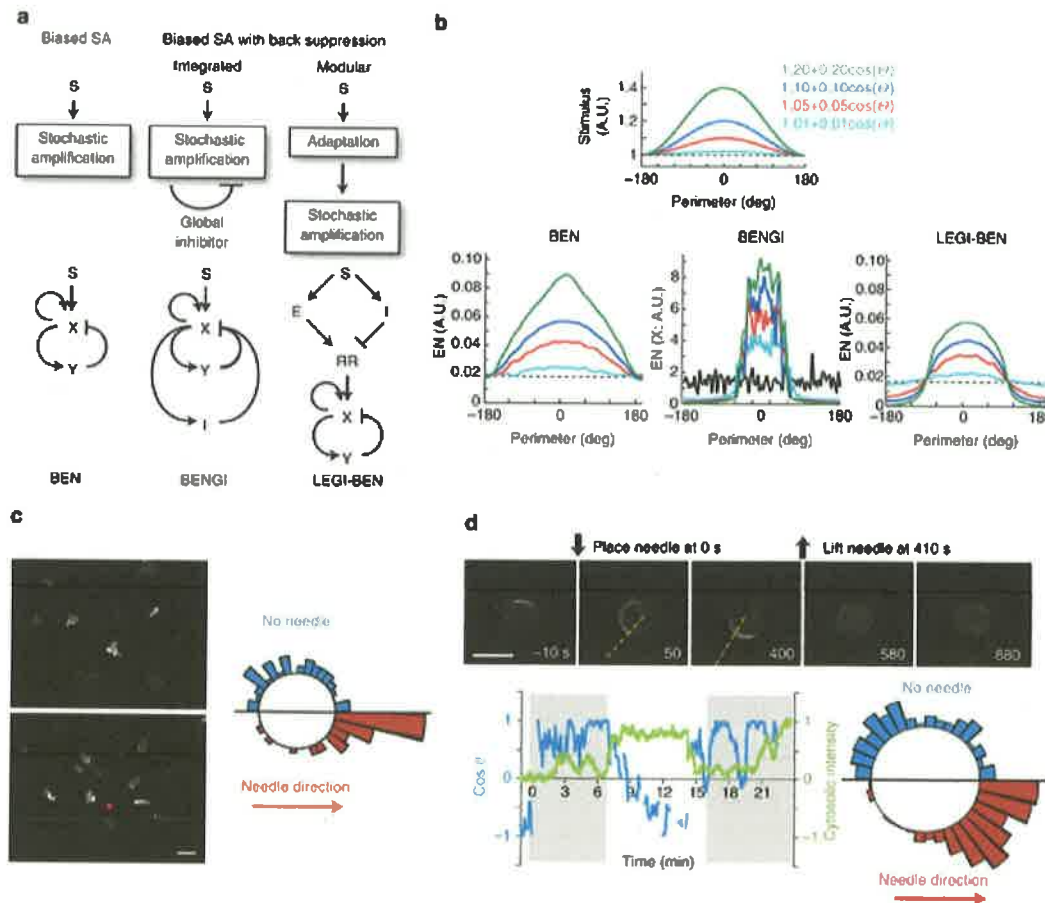
We next examined directed migration in cells lacking these pathways. Although PI3K inhibition was overcome by exposing cells to steep gradients³³, the inhibition of multiple pathways caused much stronger defects. For the majority of cells the chemotactic speed and index were reduced to 10% and 22%, respectively (Fig. 1b and Supplementary Fig. 1b). However, cells in the steepest gradients (within two cell lengths of the tip of the micropipette) did display chemotaxis. Kortholt *et al.*³⁴ have reported that cells lacking sGC in addition to PLA2, TorC2 and PI3K required 200-fold steeper gradients than wild-type cells to attain the same chemotactic index. We examined their cells and our observations concurred with theirs, although we also observed a large reduction in chemotactic speed, which they did not report (Supplementary Fig. 1c)

To examine whether blocking three pathways eliminates directional sensing, we treated wild-type or LY-treated *plaA*–/*piaA*– cells with latrunculin A, and observed Ras binding domain (RBD) crescent formation as we changed direction of the chemoattractant gradient. As shown in Fig. 1c, *plaA*–/*piaA*– cells treated with LY can respond to gradient changes as quickly as wild-type cells, but the intensity of the crescent is weaker than that of the wild-type cells. Furthermore, there are occasional activities on the low side of the gradient, not observed in wild-type cells. Taken together, the observations suggest that STEN is not required for directional sensing. However, it reads out the receptor-mediated directional sensing and couples it to movement. Therefore, we focused our investigation on the behaviour of STEN in response to temporal and spatial stimuli to elucidate the mechanisms of regulation.

Models of directional sensing in migrating cells

Most models that can account for the stochastic protrusions observed in randomly migrating cells contain a 'stochastic amplification' (SA) module. This is typically implemented as a biased EN (BEN) composed of coupled positive and delayed negative feedback loops. The positive loop amplifies local activities triggered by noise or external stimuli, whereas the negative feedback limits the life-time of protrusions. Chemotaxis is achieved through spatially promoting or suppressing SA by directional cues. Although models differ in details, they can be categorized into three general classes (Fig. 2a). In the simplest class, the SA module at each element around the cell is independently biased by the local level of chemoattractant so that activity is highest on the side facing the stimulus^{7, 8, 9, 10, 35}. The other classes of models contain a global inhibitor to suppress the activities in the back. One class of back suppression models integrates the global inhibitor into the SA module^{26, 28, 36}. We designate this class of models as BEN with global inhibitor (BENGI). In the prototype of the model, first proposed by Meinhardt²⁶, the global inhibitor acts to quickly suppress the generation of protrusions at other sites. The cells are thus intrinsically polarized, and chemoattractants work by biasing the probability of protrusion generation around the cell. In the other class of back suppression models, the chemotactic signal is first processed by an adaptive module, which subsequently biases the SA module to restrict the generation of activities to the high side of the gradient^{27, 29, 30}. In contrast to BENGI models, the global inhibitor does not depend on the activity of the SA module. We designate this class of models as LEGI-BEN. An example, which uses an incoherent feedforward loop to explain adaptation and bias the activity of an EN, was proposed by Xiong *et al.*²⁷ All three classes of models account for the ability of cells to generate greater activities towards the high side of the gradient. However, in BENGI and LEGI-BEN but not BEN models, the activities over the low side of the gradient are suppressed (Fig. 2b) and are transient when cells are exposed to uniform stimuli (see below).

Figure 2: Models of directional sensing in migrating cells and back suppression in a gradient.



(a) Three classes of models of directional sensing in migrating cells involving a stochastic amplification module (see text). The representative schemes of the three classes of models are shown below. (b) Steady-state profile of the simulated activities of the three schemes under spatial gradients of varying steepness. (c) Left: representative images of migrating *Dictyostelium* cells expressing LimE-RFP in the absence (top) or presence (bottom) of cAMP gradient. Right: circular histogram showing frequency of LimE patches with or without a gradient. Scale bar, 10 μ m. (d) Top: frames from a time-lapse video of a *Dictyostelium* cell expressing PH-GFP treated with 5 μ M latrunculin. Dotted lines indicate the direction of the tip of a cAMP-filled micropipette. Scale bar, 10 μ m. The cosine angle between the direction of the PH activity and that of the micropipette tip is plotted on the lower left graph (blue line), along with the cytosolic fluorescence intensity normalized to the pre-stimulus level (green line). Shaded grey regions indicate durations of cAMP gradient. Bottom right: circular histogram showing frequency of PH patches from 4 cells (derived from 300 frames for 'no needle' and 510 frames for 'with needle').

Suppression at the low side of the gradient

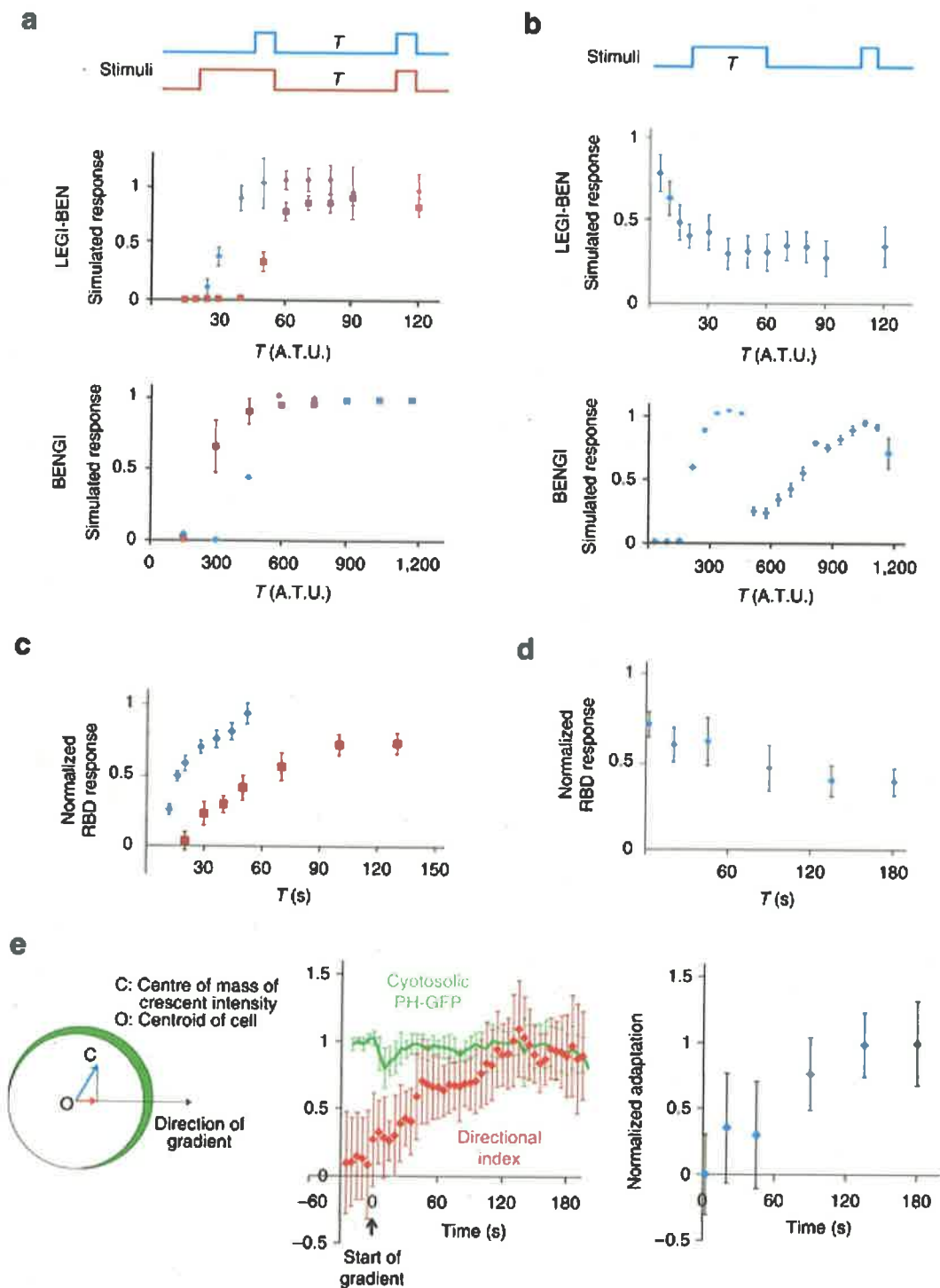
To test experimentally whether activities are suppressed at the rear, we assessed the spontaneous production of patches of LimE-RFP, which detects newly polymerized actin³⁷, on projections in cells moving in the absence or presence of a chemotactic gradient (Fig. 2c). In randomly migrating cells, the distribution of angles of patches was uniform, whereas cells moving chemotactically extended fewer projections away from and more towards the gradient. Similarly, in latrunculin-treated cells, the PIP3 (phosphatidylinositol (3,4,5)-trisphosphate) patches were suppressed at the low, and enhanced at the high, side of the gradient (Fig. 2d). These experimental results indicate that BEN models without a global inhibitor cannot adequately explain the responses of chemotactic cells.

Kinetics of responses are consistent with LEGI-BEN

To distinguish the LEGI-BEN and BENGI models, we considered the kinetics of the inhibitor under persistent stimulation and simulated the Xiong *et al.*²⁷ and Meinhardt²⁶ models under various protocols. First, we varied the interval between an initial stimulus of short or long duration and a test stimulus. Both models displayed an absolute refractory period during which the test

stimulus did not elicit a response. Lengthening the interval led to a recovery of responsiveness (Fig. 3a,b and Supplementary Fig. 2a,b). In LEGI-BEN, the longer initial stimulus delayed recovery of responsiveness to the test stimulus (Fig. 3a, upper, and Supplementary Fig. 2b). In striking contrast, in BENGI the longer initial stimulus accelerated the recovery of responsiveness to the test stimulus (Fig. 3a, lower). The difference can be traced to the way the global inhibitors are regulated: in LEGI-BEN the inhibitor depends on the stimulus and rises to a plateau during continued stimulation, whereas in BENGI the inhibitor is derived from the response, so it rises and falls as the latter adapts to the various stimuli. Thus, lengthening the initial stimulus increases the level of the global inhibitor in LEGI-BEN, but has the opposite effect in BENGI (Supplementary Fig. 2a,b,d). Second, we fixed the interval between an initial stimulus of increasing duration and a brief test stimulus. Again, there is a dramatic difference in the behaviour of the two models due to the differential regulation of the global inhibitors. In LEGI-BEN, the response to the test stimulus was initially high and decreased monotonically until the inhibitor reaches the plateau (around $T=30$ A.T.U. in upper panel of Fig. 3b, see also Supplementary Fig. 2c). In BENGI, the response to test stimulus was initially negligible and then increased (Fig. 3b, lower). Thereafter, the latter underwent a series of oscillations induced by secondary firings of the EN (Fig. 3b and Supplementary Fig. 2d).

Figure 3: Double stimulation protocols reveal distinct kinetics of adaptive and excitable networks.



(a,b) Simulated response of LEGI-BEN (upper panels) and BENGI (lower panels) to consecutive pulses with variable timing. (a) Short (2 arbitrary time unit (A.T.U.) in LEGI-BEN and 30 A.T.U. in BENGI) (blue) or long (150 and 2,250 A.T.U., respectively) (red) pulses were followed by a variable period with no stimulus, and a short (2 and 30 A.T.U., respectively) second pulse. (b) The first pulse of varying duration (T) is followed by a period (50 and 300 A.T.U., respectively) with no stimulus, and a second short pulse. The graphs in panels a and b show the height of the response to the second pulse relative to that of the first. Error bars indicate s.d. from $n=20$ simulations, each. (c,d) Ras activation in developed *Dictyostelium* cells responding to consecutive pulses of cAMP with variable timing. Stimulation protocols for c and d are the same as those used in a and b, respectively. In c, the first stimuli were 2s (blue) and 150s (red), respectively. In d, the interval between two stimuli was fixed at 50s. The graphs show the magnitude of the RBD response, defined as the peak decrease in cytosolic RBD-GFP, to the second pulse (2s) relative to that of the first. Error bars indicate s.e.m. of $n=30$ (blue) and 15 (red) cells for c and s.e.m. of $n=12$ cells for d from 2 independent experiments, respectively. (e) Comparison of kinetics of directional sensing and adaptation. Left: directional index is defined as the projection (red arrow) of the vector (green arrow, OC) from the centroid of the cell (O) to the centre of mass of crescent fluorescent intensity (C) in the direction of the gradient. Middle: temporal profile of the directional index (red)

and the mean cytosolic PH-GFP normalized to pre-stimulus level (green). A micropipette containing cAMP was introduced at 0 s. Error bar=s. d. of $n=10$ cells from three independent experiments. Right: kinetics of adaptation derived from (d). The values are normalized to the difference between the minimal and maximal levels of RBD responses.

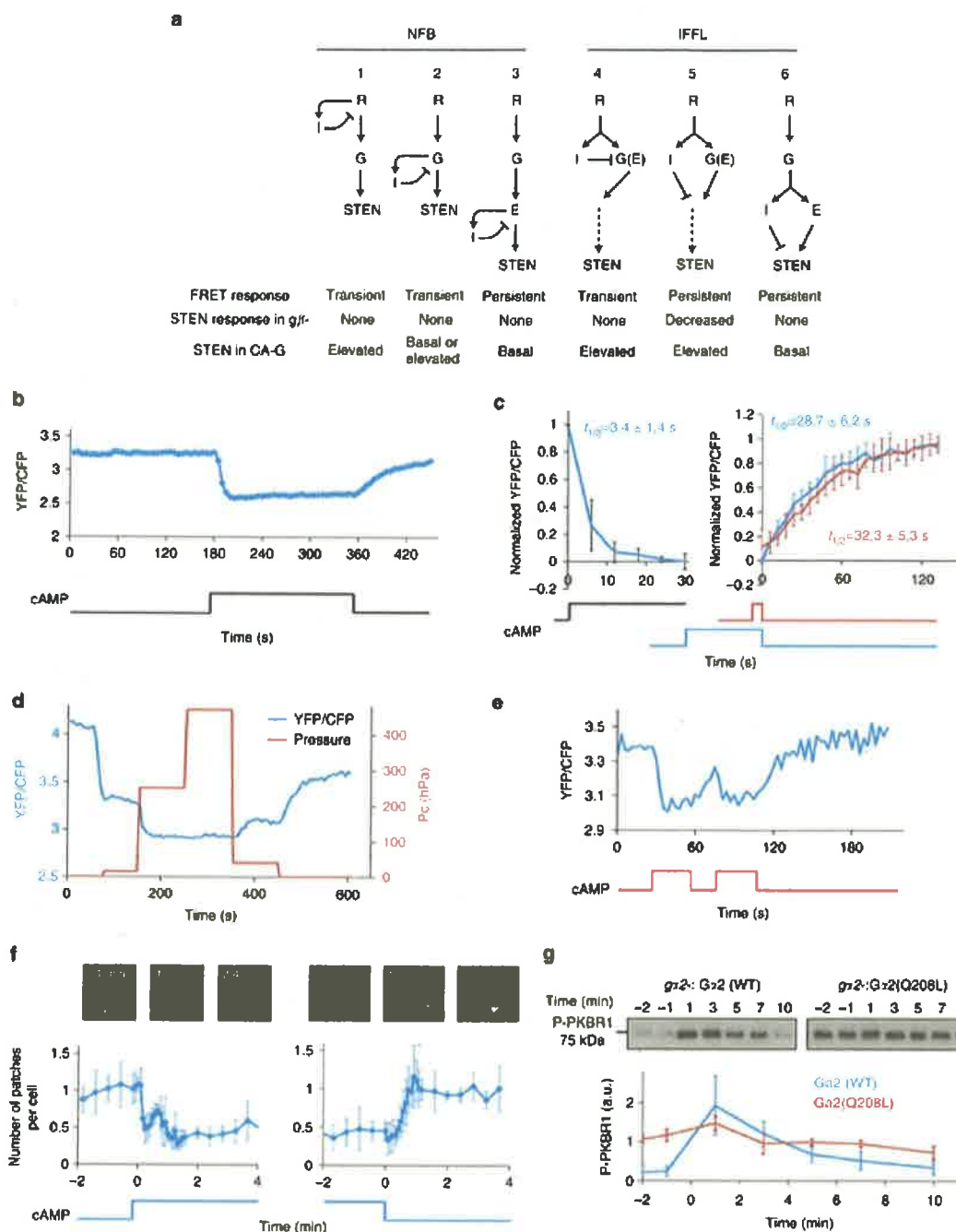
To distinguish experimentally between the two models, we carried out the double stimulation experiments in *Dictyostelium* cells expressing RBD-GFP. First, we compared the rate of recovery after a short (2 s) or long (150 s) initial stimulus. As shown in Fig. 3c, in cells adapted to the long initial stimulus, the recovery is delayed. Second, we increased the duration of the initial stimulus while keeping the recovery interval fixed at 50 s, to allow the refractory period to resolve. As shown in Fig. 3d, the response to the test stimulus decreased as the duration of the initial stimulus was increased from 10 s to 3 min. These results support the LEGI-BEN model and rule out BENGI.

As it suppresses activities at the low side, the timing of the global inhibitor in each model also dictates the response to gradients. In BENGI, the global inhibitor is fast compared with the negative feedback in the EN to suppress activities away from the high side of the gradient before they become self-catalytic²⁶. In LEGI-BEN, the inhibitor, and therefore the directional response, develop slowly. As shown in Fig. 3e, when the gradient was first applied to cells there was a global response that was followed by the gradual appearance of a crescent in the direction of the gradient. This timing matched that of adaptation determined from the double stimulation experiments. Again, this result supports LEGI-BEN and rules out BENGI.

The role of G-proteins in the LEGI module

Having found experimental evidence for LEGI-BEN, we next investigated the architecture of the LEGI module. Although we implemented LEGI as an incoherent feedforward mechanism, directional sensing and adaptation could also be achieved with a negative feedback loop^{38, 39}. We considered three possible negative feedback and three incoherent feedforward loops in which the inhibitor acts at different points relative to the G-protein (Fig. 4a). For each topology we considered (1) the kinetics of chemoattractant-mediated G-protein activation, (2) the response of STEN to chemoattractant in the absence of G-protein function and (3) the effect of constitutive G-protein activation (Fig. 4a). We carried out experiments to test these predictions.

Figure 4: Architecture of the LEGI module.



(a) Network topologies that achieve adaptation through negative feedback loops (1–3) or incoherent feedforward loops (4–6). The predicted responses of G-protein FRET to continued stimulation, the response of STEN to stimulation in *gβ*-cells, as well as the effect of constitutive activation of G-protein (CA-G) on STEN, are shown at the bottom. (b) Representative response of single-cell G-protein FRET. The ratio between emissions of *Gα2*-Cerulean (CFP) and *Gβ*-Venus (YFP) was used as surrogate readout for FRET. (c) Kinetics of G-protein FRET in response to cAMP stimulation and removal. The YFP/CFP ratio was normalized to pre-stimulus levels. Left: response to cAMP stimulation (mean±s.d. of *n*=7 cells). Right: comparison of FRET recovery after removal of short stimuli (10 s; red, mean±s.d. of *n*=12 cells) or long stimuli (90–180 s; blue, mean±s.d. of *n*=5 cells stimulated for 90, 135, 135, 120 and 180 s, respectively). The half-times were obtained by fitting data sets to exponential curves by non-linear least square method using Gnuplot (<http://www.gnuplot.info/>). (d) Representative example of graded G-protein FRET response of a single *Dictyostelium* cell to changing levels of cAMP. The YFP/CFP ratio was plotted along with the compensation pressure (*P_c*) applied to a cAMP-filled micropipette used to deliver the stimulus. (e) Representative example of G-protein FRET response to two 30 s stimuli separated by 15 s. (f) Responses of *gβ*-cells to cAMP. *gβ*-Cells expressing *LimE*-RFP and cAR1 were developed for 5.5 h before stimulation with 1 μM cAMP in ibidi chamber (<http://ibidi.com/>). Representative cell images (top) and quantification of number of patches per cell (below, mean±s.d. of *n*=4 experiments) are shown. (g) Constitutively active G-protein leads to persistent phosphorylation of PKBR1. Top: developed *ga2*-cells expressing cAR1 and either wild-type *Gα2* or *Gα2*(Q208L) were stimulated with 1 μM cAMP at 0 min. Samples were taken at indicated time points and probed with anti-

phospho-PKC antibody⁶¹. Bottom: quantitative densitometry of phosphorylated **PKBR1** normalized to the average intensity of the **Gα2(Q208L)** samples (mean±s.d. of $n=4$ experiments).

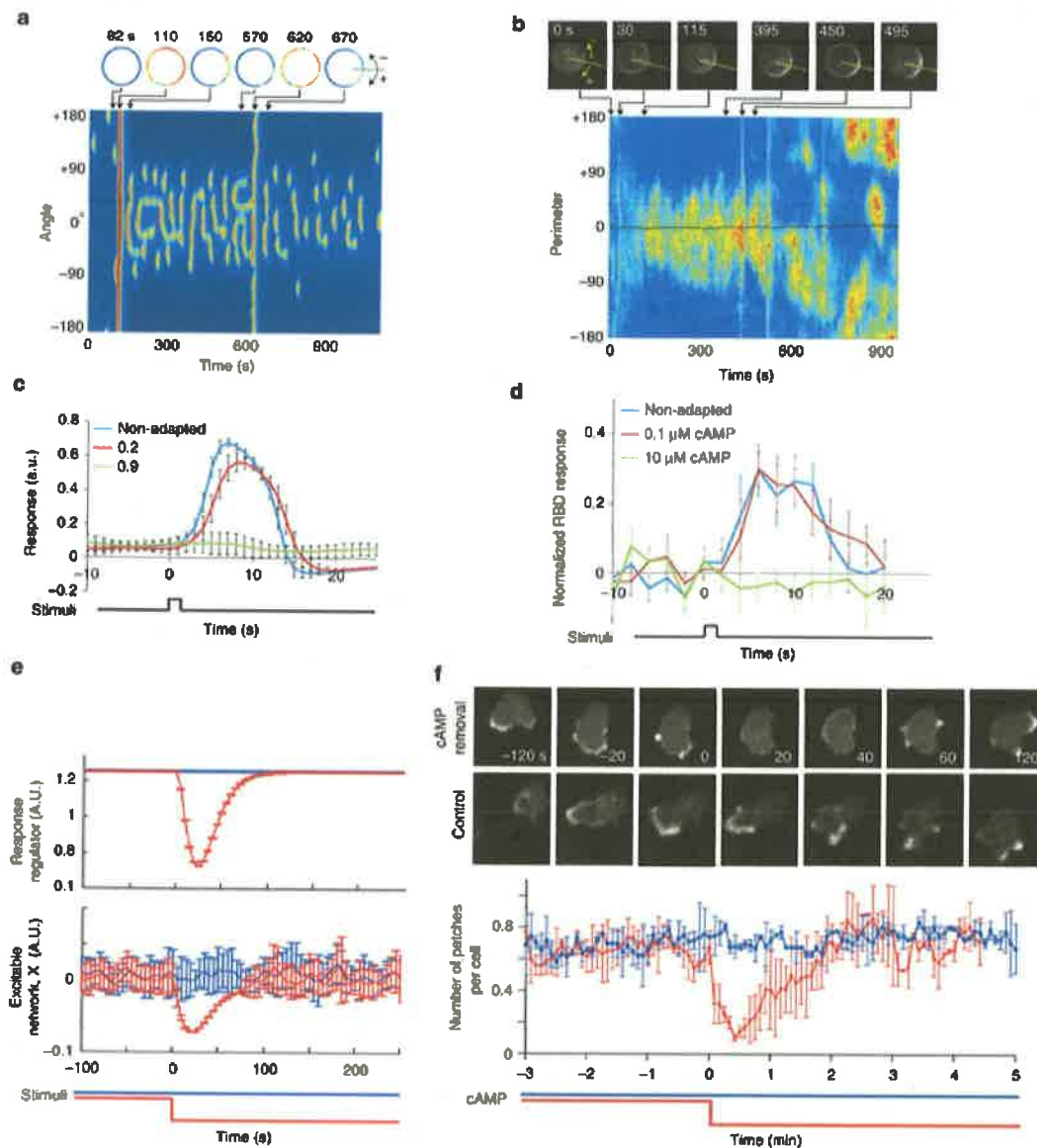
First, at the single-cell level, G-protein activation, monitored by the loss of fluorescence resonance energy transfer (FRET) between **Gα2-CFP** and **Gβ-YFP**⁴⁰, was persistent (Fig. 4b). Interestingly, loss of FRET occurred with a half-time of ~3 s, whereas the recovery of FRET after removal of stimulus occurred at a slower rate, with a half-time of ~30 s. The latter was independent of the duration of the stimulus (Fig. 4c), in contrast to recovery kinetics of RBD responses (Fig. 3c). Thus, re-association of G-protein subunits cannot account for the pattern of recovery from adaptation. Furthermore, the response was graded as the stimulus was increased (Fig. 4d) and was triggered immediately when the stimulus was removed for 15 s and reapplied (Fig. 4e). Together, these results suggest that G-protein dissociation neither adapts nor displays excitable behaviour, ruling out topologies 1, 2 and 4.

Second, we stimulated **gβ**- cells expressing **LimE-RFP** with chemoattractant. As shown in Fig. 4f, the number of patches of **LimE-RFP** gradually decreased and remained low during persistent stimulation. The cells became less motile, extended fewer projections and rounded up (Supplementary Fig. 3a). When the stimulus was removed, the pre-stimulus behaviour gradually resumed. This result can only be explained by topology 5, which allows a G-protein-independent inhibitory signal to affect STEN and downstream events. Consistently, the kinetics of **LimE-RFP** decrease is similar to those of directional sensing and adaptation (Fig. 3e). To further test topology 5, we examined the effect of a constitutively active mutant, **Gα2(Q208L)**. Although **ga2**- cells expressing the wild-type **Gα2** responded transiently to **cAMP** stimuli, there was a persistent, non-adapting elevation of phosphorylated **PKBR1** in cells expressing **Gα2(Q208L)** (Fig. 4g, see also Supplementary Fig. 3b–f). Taken together, these results suggest that the transient response to chemoattractant is mediated by an incoherent feedforward mechanism involving G-protein activation and G-protein-independent inhibition.

Responses of the signalling network in immobilized cells

Chemotactic cells are able to sense shallow gradients in the face of increasing ambient concentrations of chemoattractants. The LEGI-BEN scheme effectively accounts for this behaviour, because excitation and inhibition are specified by the current level of the stimulus and balance each other at steady state. We compared simulated and experimental results to explore this property. First, on the initial addition of a gradient, the simulation generated a global response before settling to dynamic activity towards the high side. Addition of a higher stimulus generated another transient global response followed by biased stochastic activities (Fig. 5a and Supplementary Fig. 4a). Experimentally, when immobilized cells were exposed to chemotactic gradients, PIP3 accumulation displayed similar patterns of global accumulation and dynamic patches (Fig. 5b and Supplementary Fig. 4b). Second, the simulation predicted that a brief stimulus would trigger the same response in cells fully adapted to a steady level of chemoattractant as it does in naive cells (Fig. 5c). As shown in Fig. 5d, in cells pretreated with 100 nM **cAMP** a test stimulus elicited the same response as untreated cells. The absence of response observed following pretreatment with the saturating stimulus is expected, as the test stimulus produced no further increase in receptor occupancy.

Figure 5: LEGI-BEN model accounts for response to chemoattractants of immobilized cells.



(a) Simulated activity of LEGI-BEN. The gradient (highest concentration at perimeter 0° in kymograph) was introduced at 100 s. At 600 s, the stimulus was increased globally while maintaining the spatial gradient. Snapshots of cell activity are shown above. The plotted activities are those of Y in the EN; plotting X shows similar results²⁷. (b) Kymograph showing 'dancing' crescents of a latrunculin-treated *Dictyostelium* cell expressing PH-GFP. A gradient was initiated at 15 s, and global stimuli of 1 nM, 10 nM and 100 nM cAMP were added at 450, 540 and 730 s, respectively. The plotted activities in kymograph reflect the ratio of local cortical PH-GFP to mean cytosolic intensity. Note that after addition of 10 nM cAMP, the PH-GFP crescents were no longer biased as the gradient generated by the micropipette became negligible. In snapshots of cells (top), the direction of gradient was indicated by dotted lines. (c) Simulated responses (mean \pm s.d. of the level of X, the activator in the EN, for $n=10$ simulations) of LEGI-BEN to a short (2 s) pulse of magnitude 1 AU, assuming prior stimulus levels (basal, 0.2 and 0.9 A.U.). (d) Decrease in cytosolic RBD (mean \pm s.d. for $n=8$ cells) in developed *Dictyostelium* cells (immobilized with 5 μ M latrunculin A) in response to a short cAMP stimulus with or without prior adaptation to indicated cAMP concentration for 3 min. (e) Simulation of stimulus removal in LEGI-BEN. The system was allowed to reach steady state before the stimulus was removed at 0 s (red) or continued (blue). Shown are the responses of the LEGI response regulator and EN (mean \pm s.d. of $n=10$ simulations). (f) LimE-RFP response to removal of stimulus. *Dictyostelium* cells were incubated in 50 μ L DB buffer containing 0.1 μ M cAMP for 6 min followed by dilution with 20 \times volumes of buffer without (cAMP removal) or with 0.1 μ M cAMP (control). Top: snapshots from time-lapse videos. Scale bar, 10 μ m. Bottom: quantification of LimE activity (mean \pm s.d. of $n=50$ cells; 3 experiments) in cAMP removal (red) and control (blue) experiments.

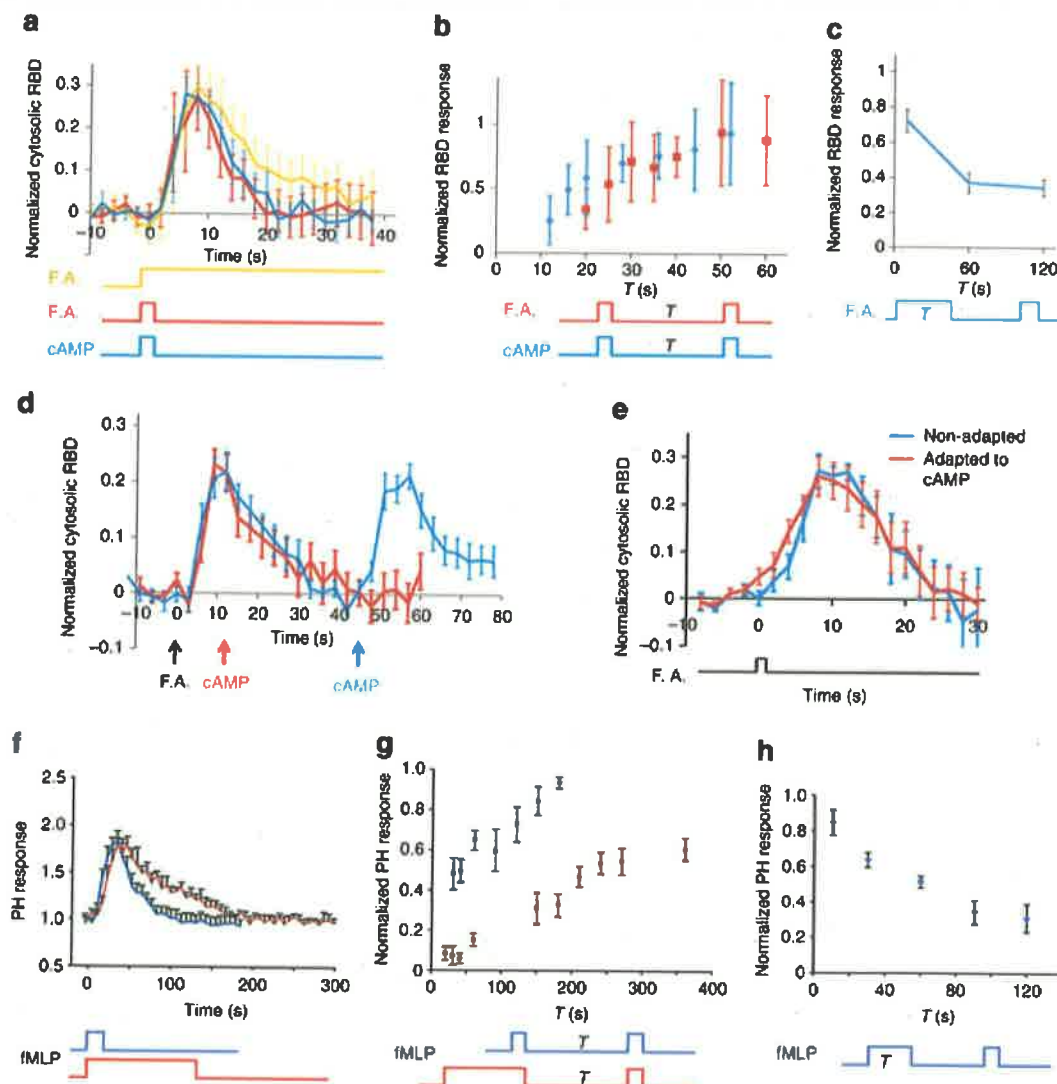
According to the LEGI-BEN model, removal of a uniform stimulus will lead to transient suppression of the STEN activity: The inhibitor drops more slowly than the excitor and the level of the response regulator transiently dips below its basal level (Fig. 5e).

To test this, we pretreated cells expressing **LimE-RFP** with **cAMP** for ~6 min and then suddenly removed the stimulus (Fig. 5f). The addition of the stimulus generated the typical series of responses and then the cells resumed pre-stimulus behaviour after 5 min. When the stimulus was removed, **LimE-RFP** disappeared from the membrane for an extended period and the cells retracted. Then, the cells gradually resumed random migration with **LimE-RFP** appearing on protrusions. Similar transient suppression was observed for RBD, indicating this behaviour reflects the inhibitory effect of LEG1 on STEN (Supplementary Fig. 4e).

LEGI-BEN in response to different chemoattractants

The experiments shown so far were carried out in developed *Dictyostelium* cells stimulated with **cAMP**. To test whether the LEGI-BEN model also accounts for responses to other chemoattractants, we carried out **folic acid** stimulation in less differentiated cells. These cells are chemotactic towards both **folic acid** and **cAMP**. The profiles of responses to **folic acid** were remarkably similar to those induced by **cAMP** (Fig. 6a). First, the responses to short and long **folic acid** stimuli were nearly identical. Second, when cells were stimulated with two brief **folic acid** stimuli separated by increasing durations, they displayed nearly the same refractory period (Fig. 6b). Third, cells pretreated with longer initial stimuli were less responsive to second stimuli (Fig. 6c), suggesting that adaptation also occurs for **folic acid** responses.

Figure 6: LEGI-BEN for folic acid in *Dictyostelium* and fMLP response in human neutrophils.



(a–c) Ras activation in *Dictyostelium* cells stimulated with **folic acid**. (a) Responses ($n=32$ cells each) to 2 s (red) and long (orange) stimuli. The response to a 2 s **cAMP** stimulus ($n=10$ cells, blue) is plotted for comparison. (b) Responses ($n=15$ cells, red) to the second 2 s stimulus applied after variable intervals (T) following the first 2 s stimulus. The response to **cAMP** stimuli ($n=30$ cells, blue) is plotted for

comparison. (c) Responses ($n=20, 19, 18$ cells, respectively; 3 experiments) to a 2 s **folic acid** stimuli applied 50 s after first stimuli of 10, 60 and 120 s. (d) Ras activation in *Dictyostelium* cells stimulated with 5 μM **folic acid** at 0 s followed by 0.3 μM **cAMP** at 12 s (red, $n=15$ cells; 4 experiments) or 45 s (blue, $n=13$ cells; 5 experiments). (e) Ras activation in *Dictyostelium* cells responding to **folic acid** with or without prior adaptation to **cAMP**. Non-adapted cells were stimulated by 2 s **folic acid** (blue). The same cells were then treated with 200 μM **cAMP** for 3 min and stimulated with a 2 s **folic acid** pulse (red; $n=12$ cells; 2 experiments). For a–e, responses were defined as the peak cytosolic RBD-GFP decrease normalized to the pre-stimulus cytosolic levels (a,d,e) or to the first response (b,c). (f–h) PH-GFP responses in human HL60 neutrophils responding to **fMLP**. (f) Responses ($n=4$ cells each) to 10 s (blue) and 120 s (red) stimulation. (g) Responses ($n=5$ cells each) to a second 10 s stimulation administered after various intervals (T) following first stimuli of 10 s (blue) or 120 s (red). (h) Responses ($n=5$ cells each) to a second 10 s stimulation administered 150 s after removal of the first stimulation of various durations (T). In all experiments, HL-60 cells were immobilized with the JLY cocktail (see Methods)⁶⁰. The responses were defined as peak changes in the (membrane+cytosol)/(cytosol) of PH grey values. For g and h, normalization was to the responses to the first stimuli. Error bars: s.d. for a,b and s.e.m. for c–h.

To determine whether **cAMP** and **folic acid** activate the same EN and whether adaptation to one causes adaptation to the other, we paired stimuli. First, cells responded to both **folic acid** and **cAMP** stimuli that were separated by 45 s (Fig. 6d, blue line), but when the separation was 12 s, the second response did not occur (Fig. 6d, red). Thus, cells do not respond to **cAMP** during the refractory period induced by **folic acid**. Second, we pretreated the cells with 10 μM **cAMP** for 3 min and then applied a brief **folic acid** stimulus. The **folic acid** stimulus elicited a response similar to that observed in untreated cells (Fig. 6e and Supplementary Movie 1). Taken together, these results suggest that the same STEN is activated by the two stimuli, but that cells adapted to one can still respond to the other.

Conservation of LEGI-BEN scheme in human neutrophils

We next tested whether the features of LEGI-BEN are conserved in HL-60 neutrophils, derived from the human promyelocytic leukemia cell line. Immobilized neutrophils displayed dynamic flashes of PH-Akt-GFP that were 2–5 μm in diameter and lasted 50–150 s (Supplementary Fig. 5a–c and Supplementary Movie 2). The membrane marker C5aR-RFP did not show changes in intensity. Several other tests also indicated that the signalling activities are excitable. First, 10 and 120 s **fMLP** stimuli induced responses with the same rise time and peak magnitude (Fig. 6f), and as in *Dictyostelium* the response to the longer stimulus had a slower declining phase. Second, with two short (10 s) stimuli separated by increasing intervals, the second response showed a gradual recovery when the interval between stimuli was increased (Fig. 6g, blue). Taken together, the spontaneous flashes, 'all-or-nothing' responses to short stimuli, and the refractory period suggest that signal transduction activities in neutrophils are excitable.

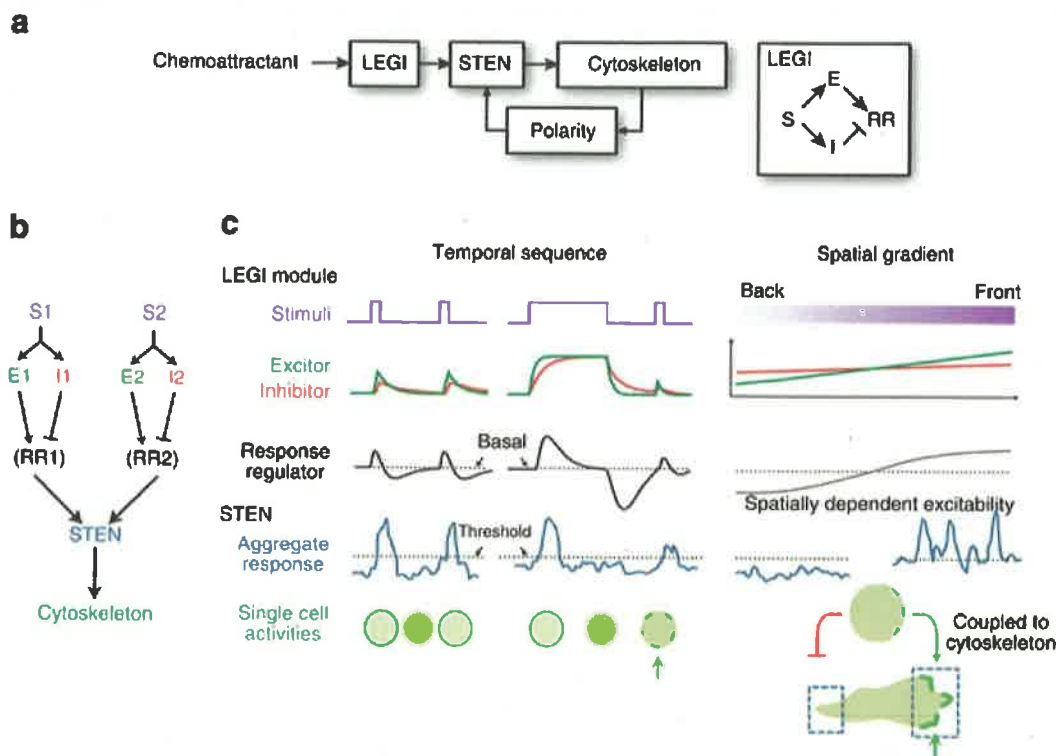
Using the protocols outlined in Fig. 3, we tested whether HL-60 cells display adaptation. First, when the interval between adapting and test stimuli was fixed, increasing the duration of the adapting stimulus diminished the response to the test stimulus (Fig. 6h). Second, in cells pretreated with short or long initial stimuli, the long pretreatment delayed the subsequent rate of recovery (Fig. 6g, red). Together, these results suggest that responses of HL-60 cells, as in *Dictyostelium* cells, are consistent with the predictions of the LEGI-BEN model.

Discussion

A number of theoretical models have attempted to explain the remarkable ability of chemotactic cells to detect and migrate along very shallow chemoattractant gradients, even in the presence of high background levels (reviewed in ref. 41). We have focused our attention on models that incorporate stochastic activities, as many investigators have noticed that the signal transduction and cytoskeletal activities display features of excitability such as spontaneous patches and propagating waves^{27, 31, 42, 43, 44, 45, 46, 47}. In this study, we provided evidence favouring the LEGI-BEN model over other existing schemes. First, we ruled out models that do not incorporate back suppression, as the spontaneous activation of Ras and PI3K are repressed at the back of the cells in a gradient. Second, we ruled out models that integrate a global inhibitor into the EN based on the pattern of responses to paired stimuli. Our evidence suggests that the adaptive module involves a G-protein-dependent excitor and -independent inhibitor forming an incoherent feedforward mechanism. A feedforward mechanism has been proposed for the kinetic of Ras

activation by Takeda *et al.*¹⁴, although the conclusion was drawn from analysing the termination of responses within 30 s of stimulation, before adaptation was complete (Fig. 3d). Note that the LEGI-BEN scheme we present here does not take into account polarity, which is seen in non-stimulated, randomly migrating cells. Rather, it focuses on the role of directional sensing in regulating STEN. A complete model involving LEGI, STEN, cytoskeleton and polarity is shown in Fig. 7a (ref. 48).

Figure 7: Summary of responses of LEGI-BEN to temporal and spatial stimuli.



(a) Modular view of the chemotaxis signalling pathway. The LEGI module senses chemoattractant stimuli and biases the activity of the STEN, which regulates the cytoskeleton. Polarity, which depends on the existence of an intact cytoskeleton, provides feedback by further biasing the STEN's activity⁴⁸. The LEGI module (right) includes excitor (E) and inhibitor (I) elements that are regulated by receptor occupancy (S) and regulate the response regulator (RR) in complementary ways. (b) Response to multiple stimuli. Chemoattractants S1 and S2 activate different LEGI modules, which in turn regulate the same STEN that is coupled to the cytoskeletal network to mediate chemotaxis. (c) Summary of responses to temporal sequences and spatial gradients of chemoattractant. On the left, two stimuli separated by an interval trigger rapid changes in the excitor and slower changes in the inhibitor, which control the level of the response regulator. When the level of the response regulator crosses the threshold, it triggers the activation of STEN, which is all-or-none for each element on the membrane but may not be uniform across the whole cell (arrows)³¹. In a stable gradient, the excitor and inhibitor are generated by the local level of receptor occupancy, but as the inhibitor has a larger dispersion range (determined by its diffusion rate and half-life⁶³) its steady-state distribution is shallower than that of the excitor. Consequently, the response regulator is higher than the threshold at the front and lower than the threshold at the back. This promotes persistent STEN activity at the front and when coupled to the cytoskeleton biases migration.

Activities involving multiple signal transduction pathways are critical for chemotaxis^{34, 49} and cells can still chemotax with disruption of individual pathways^{50, 51, 52}. We have shown previously that cells with disruptions in multiple pathways do not move in the absence of chemoattractant³¹. Here we found that blocking multiple pathways prevents actin polymerization in response to chemoattractant. Furthermore, these cells cannot carry out chemotaxis, because they do not move unless exposed to extremely steep chemoattractant gradients. Independent cell lines created in different laboratories with multiple signal transduction pathways disrupted displayed similar behaviour. Although the STEN is required for chemotaxis, its excessive activation impairs the process^{48, 53}. Consistent with Veltman *et al.*⁵², we found that treatment with a low-dose LY improved chemotaxis of partially developed cells (Supplementary Fig. 1d), which, in the absence of LY, display more spontaneous patches of PH-GFP compared

with more developed cells (Supplementary Fig. 1e).

Although the LEGI inhibitor is unknown, our results indicate that it is generated by occupancy of the receptor and independently of the G-protein. First, stimulation of cells lacking the $G\beta$ subunit elicits no response, only a slowly developing suppression of basal cytoskeletal activity and pseudopod extension, which is reversed on removal of the stimulus. Second, constitutively active $G\alpha$ generated a persistent, non-adapting increase of **PKBR1** phosphorylation, indicating that adaptation is not derived from G-protein activation. We did not observe a robust negative effect of stimulation in these cells, presumably because the activity is too strong to suppress. Third, when a cell has been adapted, removal of the stimulus causes suppression of basal RBD and cytoskeletal activity (Fig. 5f). We speculate that the inhibitor decays more slowly than the excitor and this sends a negative signal to the STEN. Clearly, these features of adaptation as well as the fact that loss of G-protein FRET persisted as long as the stimulus was present are inconsistent with current models in which receptor phosphorylation uncouples interaction with G proteins⁵⁴.

We provided evidence that two chemoattractants for *Dictyostelium*, **folic acid** and **cAMP**, activate the same STEN but they have distinct directional sensing adaptive networks. Even though **folic acid** and **cAMP** act through **Gα4** and **Gα2** (refs 55, 56), respectively, **cAMP** does not induce a response during the refractory period induced by **folic acid**. In addition, we extend earlier observations that *Dictyostelium* cells adapted to either **folic acid** or **cAMP** remain responsive to the other chemoattractant⁵⁷. By examining the responses at the single cellular level, we prove that this phenomenon occurs in individual cells and is not due to heterogeneity in responsiveness to **cAMP** and **folic acid** in different subsets of cells. We speculate that different chemoattractants in general activate the STEN through different LEGI modules (Fig. 7b), although some components of the LEGI may be shared.

The response of STEN to combinations of temporal and spatial stimuli can be explained by the LEGI-BEN model (Fig. 7c). First, it can explain the responses to paired stimuli. The example shown in the figure illustrates the behaviour of LEGI and STEN during the protocol designed to measure the time course of adaptation (Fig. 7c, left). A brief initial stimulus has little effect on the test stimulus separated by a sufficient interval, so that the response regulator causes STEN to cross the threshold equally. However, a longer initial stimulus generates inhibitor, which has not dissipated when the test stimulus is applied; thus, the amount of response regulator generated barely allows the STEN to cross threshold. Similar diagrams can explain the protocol for monitoring deadaptation. Remarkably, these features of LEGI-BEN could not only explain responses of signal transduction network in *Dictyostelium* but also in human neutrophils, suggesting an evolutionarily conserved mechanism for eukaryotic chemotaxis. Second, the LEGI-BEN model explains how spatial gradients of chemoattractant can bias the STEN (Fig. 7c, right). In a gradient, the excitor is greater than the global inhibitor at the front and less at the back. This causes the response regulator to be above or below its basal level at the front or back, respectively. In turn, STEN activity is higher at the front and more easily crosses the threshold, while at the back it is suppressed. When the background level of chemoattractant is changed, the adaptation mechanism ensures that the response regulator returns to the same spatial profile, which keeps the system within the range of excitability of the STEN.

Methods

Cells

Wild-type *Dictyostelium discoideum* cells of the AX2 strain, obtained from the R. Kay laboratory (MRC Laboratory of Molecular Biology, UK), were used in this study. The *aca*⁻, *gβ*⁻ and *plA*⁻/*plA*⁻ cells were described previously^{31, 58, 59}. *sGC*⁻ and *sGC*⁻/*plA*⁻/*plA*⁻ cells were obtained from A. Kortholt and P. Van Haastert (University of Groningen). Cells were transformed with plasmids encoding RBD-GFP, PH-RFP, **Gα2**-CFP, **Gβ**-YFP or **LimE**-RFP by electroporation and maintained in HL-5 medium containing **G418** (20 μg ml⁻¹) or hygromycin (50 μg ml⁻¹) at 22 °C. For **folic acid** stimulation experiments, cells were washed in development (DB) buffer (5 mM **Na2HPO4**, 5 mM **KH2PO4**, 2 mM **MgSO4** and 0.2 mM **CaCl2**) and shaken in suspension for 1–2 h at a density of 2 × 10⁷ cells per ml. For **cAMP** stimulation experiments, cells were developed for 5 h by pulsing with **cAMP** every 6 min in DB buffer at a density of 2 × 10⁷ cells per ml.

HL-60 cells were cultured in RPMI 1640 containing GlutaMAX-1 (Gibco, Life Technologies, Grand Island, NY) supplemented with 20% heat-inactivated fetal bovine serum (Gibco, Life Technologies), 100 U ml⁻¹ penicillin and 100 mg ml⁻¹ streptomycin in 5% CO₂ incubator at 37 °C. Differentiation into neutrophil-like cells was induced by adding 1.3% dimethyl sulphoxide (DMSO; Sigma-Aldrich, St Louis, MO) into culture medium for 5 days. HL-60 cells were infected with FUW lentivirus (a gift from Dr Christopher Cooper in Stephen Desiderio's Lab) carrying PH-Akt-GFP or C5aR-RFP. Positive cells are selected by FACS analysis.

Microscopy

Confocal microscopy was carried out on a Leica DMI6000 inverted microscope equipped with Yokogawa CSU10 spinning Nipkow disk with microlenses and illuminated by a Kr/Ar laser.

Dictyostelium cells were transferred to Lab-Tek II chambered cover glasses (Thermo Scientific) containing DB buffer before imaging. Latrunculin A and LY294002 were diluted to the final concentration from a stock solution in DMSO (concentration: 1 mM for latrunculin A and 50 mM for LY294002). Stimulation was carried out by lowering a micropipette containing chemoattractants (10 µM cAMP or 100 µM folic acid) to the viewing field using a FemtoJet Microinjector controlled by a micromanipulator (Eppendorf). Based on the temporal profile of fluorescence from a micropipette filled with Alexa Fluor 594, the change in the concentration of chemoattractants occurs with a half-time of about 1.3 s within the viewing field. To eliminate the confounding effect of photosensitivity in adaptation, cells were not imaged during prolonged first stimulation in double stimulation experiments. Imaging of cells was started 10 s before the second stimulus was applied.

HL-60 neutrophils were spun down, washed with mHBSS medium (137 mM NaCl, 4 mM KCl, 1.2 mM MgCl₂, 10 mg ml⁻¹ glucose and 20 mM HEPES, pH 7.2), resuspended with mHBSS containing 0.2% BSA (Sigma-Aldrich) and then seeded on Lab-Tek chambered cover glasses (NUNC, Thermo Fisher Scientific, Rochester, NY) pre-coated with 100 µg ml⁻¹ human fibronectin (Sigma-Aldrich). Cells were incubated at 37 °C for 10 min, rinsed twice with mHBSS medium and then bathed in mHBSS containing 0.2% BSA before imaging. JLY cocktail treatment⁶⁰ was done by addition of Y27632 (final concentration: 10 µM), incubation for 10 min, followed by simultaneous addition of Latrunculin B and Jasplakinolide (final concentrations 5 µM and 8 µM, respectively). Stock concentrations are 25 mM for latrunculin B (in DMSO), 1 mM for Jasplakinolide (in DMSO) and 10 µM for Y27632 (in double-distilled H₂O). Stimulation was carried out by lowering a micropipette containing 10 µM fMLP to the viewing field using a FemtoJet Microinjector controlled by a micromanipulator (Eppendorf).

Fluorescence resonance energy transfer

Detailed protocol for FRET experiments has been described previously⁶¹. Briefly, FRET experiments were carried out with either an Olympus IX71 inverted microscope illuminated by a Kr/Ar laser (457 nm) source or a Nikon Eclipse TiE microscope illuminated by a diode laser (440 nm). Images were acquired by a Photometrics Cascade 512B intensified charge-coupled device camera controlled by MetaMorph (UCI) or a Photometrics Evolve electron multiplying charge-coupled device camera controlled by Nikon NIS-Elements. A Dual-View system (Optical Insights, LLC) was used for simultaneous imaging of cyan fluorescent protein (CFP) and yellow fluorescent protein (YFP) fluorescence in doubly labelled cells. The ratio between background-corrected YFP and CFP signals was used as surrogate for FRET efficiency.

Image analysis

Images were analysed with ImageJ (NIH). The responses to chemoattractant stimulation were calculated from the decrease in the mean cytoplasmic fluorescence, as described in figure legends.

The kymographs of the activities in the latrunculin-treated cells were created using the image processing toolbox of Matlab (MathWorks, Natick, MA). First, the fluorescent intensities of all frames in the movies were summed. The resultant composite image was segmented using adaptive thresholding and fitted to a circle. Thereafter, each frame of the movie was individually segmented to find the centroid of the cell at that frame. Using the calculated centroid, the intersection of a ray with circles of the given radius (±3 pixels) was computed. From this set of pixels, the maximum intensity was assigned to that angle. This was repeated for rays spaced 1° apart, creating a matrix of size 360 by the number of frames, which was then plotted as an intensity

Immunoblotting

Dictyostelium cells developed for 5–6 h were treated with 5 mM caffeine in DB buffer and shaken for 20 min. Cells were then pelleted and resuspended in cold DB buffer at 2×10^7 cells per ml. Cells were stimulated with $1 \mu\text{M}$ cAMP on ice and samples taken at various time points were lysed in SDS sample buffer. PKBR1 phosphorylation was detected as described previously⁶². Briefly, proteins were separated on 4–15% SDS–PAGE gels and transferred to polyvinylidene difluoride membranes. After blocking with 5% skim milk in TBST, the membranes were probed with anti phospho-PKC (pan) antibody (190D10 rabbit monoclonal antibody, Cell Signaling 2060, 1:2,000 dilution in TBST with 5% BSA at 4 °C for 16–20 h), followed by detection with anti-rabbit IgG-HRP (GE Healthcare Life Sciences NA934V, 1:5,000 dilution in TBST at room temperature for 1 h). An example of uncropped blot is shown in Supplementary Fig. 3f.

Computer simulation

Simulations of the coupled LEGI-BEN were carried out as described previously^{27,48}. Briefly, the LEGI mechanism is given by partial differential equations:

$$\frac{\partial E}{\partial t} = -k_{-E}E + k_E S \quad (1)$$

$$\frac{\partial I}{\partial t} = -k_{-I}I + k_I S + D_I \nabla^2 I \quad (2)$$

$$\frac{\partial R}{\partial t} = -k_{-R}R + k_R \frac{k_e + E}{k_i + I} \quad (3)$$

where S , E , I and R describe the levels of receptor occupancy, the LEGI, and response regulator, respectively. Note that the equation for the response regulator differs from those previously implemented. The parameters k_e and k_i describe basal levels of excitation and inhibition. Under spatially uniform stimulus, S_0 , the steady-state level of the response regulator is

$$R = (k_R/k_{-R}) \frac{k_e + (k_E/k_{-E})S_0}{k_i + (k_I/k_{-I})S_0} \quad (4)$$

Perfect adaptation requires that this be independent of S_0 , which can be achieved if k_e and k_i are both small relative to $(k_E/k_{-E})S_0$ and $(k_I/k_{-I})S_0$, respectively. We make this assumption and set the 'basal' level of S_0 at 0.1 A.U. Unless stated, pulses were of height 1 A.U.

The EN is implemented as an activator (X) inhibitor (Y) system, satisfying the stochastic partial differential equations:

$$\frac{\partial X}{\partial t} = k_{XX} \frac{X^2}{k_M^2 + X^2} - k_{-X}X - k_{YX}Y + k_{UX}U + D_X \nabla^2 X \quad (5)$$

$$\frac{\partial Y}{\partial t} = k_{XY}X - k_{-Y}Y + D_Y \nabla^2 Y \quad (6)$$

Both components in the EN diffuse spatially, with diffusion coefficients D_X and D_Y , respectively. The signal U , which is used to bias the activity of the excitable system, incorporates three components: a basal level of activity (B), a stochastic component (N) and a contribution from the LEGI response regulator (R). The effect of each of these is additive: $U = B + N + \lambda(R - R_{\text{init}})$. The stochastic component is modeled as zero mean, white noise process with variance one.

The simulations were carried out by solving the five differential equations using the method of lines—whereby partial differential equations are converted into ordinary differential equations by discretizing the spatial variable and approximating the Laplacian

with central differences. A one-dimensional domain with periodic boundary conditions (representing the boundary of a two-dimensional, circular cell) was discretized using 314 elements. As the LEGI mechanism is deterministic, the three equations of this subsystem were solved using the Runge-Kutta ode45 solver in Matlab. Once these solutions were obtained, the stochastic differential equations of the EN were solved using the SDE toolbox for Matlab: (<http://sdetoolbox.sourceforge.net>). Time steps were set to 0.025 s. During the simulations, all parameters used (except B , λ and R_{init}) were varied stochastically around the perimeter of the cell by selecting from a uniform distribution in the range $k(1 \pm \delta)$ where k is the nominal value of the parameter and $\delta=0.05$. Supplementary Table 1 summarizes the nominal parameters used.

Simulations for the BENGI class use the model of Meinhardt²⁶:

$$\frac{\partial X}{\partial t} = -k_{-X}X + \frac{U(X^2/I + k_X)}{(k_{MY} + Y)(1 + k_{MX}X^2)} + D_X \nabla^2 X \quad (7)$$

$$\frac{\partial Y}{\partial t} = -k_{-Y}Y + k_{XY}X + D_Y \nabla^2 Y \quad (8)$$

$$\frac{\partial I}{\partial t} = -k_{-I}I + \frac{k_I}{2\pi} \int_0^{2\pi} X(\theta) d\theta + D_I \nabla^2 I \quad (9)$$

$$U = k_U(S + k_N N) \quad (10)$$

As above, the spatial aspects were achieved through the method of lines, using a discretization of 90 points around a circle. Parameters used are as in Neilson *et al.*²⁸, which match those of Meinhardt except for small differences; for example, non-zero diffusion terms D_X and D_Y (see Supplementary Table 1). Note that the time scale of these simulations is considerably slower than either the LEGI-BEN or experiments, so that all the time intervals of Fig. 3 were modified so that the two systems had compatible dynamics.

The equations of the BENGI model were implemented in two different ways. Matlab's ode15s solver was used in the absence of noise ($N=0$). To simulate the effect of noise, we assumed that $N(t)$ was a Gaussian, white noise process with mean $1/2$ and variance $1/12$. The simulation was then run in the SDE toolbox as above. These numbers were used to match the statistics of the noise used in the Meinhardt model (which assumes a uniformly distributed random variable between 0 and 1 at each time step).

Statistical analysis and repeatability of experiments

Statistical significance and P -values were determined using the two-tailed Student's t -test. Mean values \pm either s.d. or s.e.m. were reported as indicated in figure legends.

Two independent experiments were performed for Figs 1a, 3c,d, 5d and 6a,b,h, and Supplementary Fig. 3f; three experiments for Figs 5f and 6c,f,g, and Supplementary Figs 1c, 3d and 4d; four experiments for Figs 4c,g and 6d, and Supplementary Fig. 4e; five experiments for Supplementary Fig. 1e; and six experiments for Supplementary Fig. 1a. Statistics were derived by aggregating the n numbers noted in each figure legend across independent experiments.

Representative images associated with Figs 1a, 2c,d, 4g and 5f, and Supplementary Figs 3d,f and 4d,e are shown along with statistics.

Representative images are also used for Figs 1c and 5b, and Supplementary Figs 3c,e, and 5a, which have been repeated in more than three independent experiments. Specifically, the 'dancing crescents' in Fig. 5b and Supplementary Fig. 4b were seen in all cells that expressed PH-GFP and responded directionally to cAMP gradient. Figure 1c has been repeated three times. The dynamic flashes of PH-Akt-GFP in Supplementary Fig. 5a were observed in over ten experiments.

Additional information

How to cite this article: Tang, M. *et al.* Evolutionarily conserved coupling of adaptive and excitable networks mediates eukaryotic chemotaxis. *Nat. Commun.* 5:5175 doi: 10.1038/ncomms6175 (2014).

References

1. Swaney, K. F., Huang, C. H. & Devreotes, P. N. Eukaryotic chemotaxis: a network of signaling pathways controls motility, directional sensing, and polarity. *Annu. Rev. Biophys.* **39**, 265–289 (2010).
2. Iglesias, P. A. & Devreotes, P. N. Navigating through models of chemotaxis. *Curr. Opin. Cell Biol.* **20**, 35–40 (2008).
3. Zigmond, S. H. Mechanisms of sensing chemical gradients by polymorphonuclear leukocytes. *Nature* **249**, 450–452 (1974).
4. Mato, J. M., Losada, A., Nanjundiah, V. & Konijn, T. M. Signal input for a chemotactic response in the cellular slime mold *Dictyostelium discoideum*. *Proc. Natl Acad. Sci. USA* **72**, 4991–4993 (1975).
5. Tranquillo, R. T., Lauffenburger, D. A. & Zigmond, S. H. A stochastic model for leukocyte random motility and chemotaxis based on receptor binding fluctuations. *J. Cell Biol.* **106**, 303–309 (1988).
6. Fuller, D. *et al.* External and internal constraints on eukaryotic chemotaxis. *Proc. Natl Acad. Sci. USA* **107**, 9656–9659 (2010).
7. Hecht, I., Kessler, D. A. & Levine, H. Transient localized patterns in noise-driven reaction-diffusion systems. *Phys. Rev. Lett.* **104**, 158301 (2010).
8. Whitlam, S., Bretschneider, T. & Burroughs, N. J. Transformation from spots to waves in a model of actin pattern formation. *Phys. Rev. Lett.* **102**, 198103 (2009).
9. Carlsson, A. E. Dendritic actin filament nucleation causes traveling waves and patches. *Phys. Rev. Lett.* **104**, 228102 (2010).
10. Arriumerlou, C. & Meyer, T. A local coupling model and compass parameter for eukaryotic chemotaxis. *Dev. Cell* **8**, 215–227 (2005).
11. Parent, C. A. & Devreotes, P. N. A cell's sense of direction. *Science* **284**, 765–770 (1999).
12. Levchenko, A. & Iglesias, P. A. Models of eukaryotic gradient sensing: application to chemotaxis of amoebae and neutrophils. *Biophys. J.* **82**, 50–63 (2002).
13. Levine, H., Kessler, D. A. & Rappel, W. J. Directional sensing in eukaryotic chemotaxis: a balanced inactivation model. *Proc. Natl Acad. Sci. USA* **103**, 9761–9766 (2006).
14. Takeda, K. *et al.* Incoherent feedforward control governs adaptation of activated ras in a eukaryotic chemotaxis pathway. *Sci. Signal.* **5**, ra2 (2012).
15. Tang, Y. & Othmer, H. G. A G protein-based model of adaptation in *Dictyostelium discoideum*. *Math. Biosci.* **120**, 25–76 (1994).
16. Wong, K., Pertz, O., Hahn, K. & Bourne, H. Neutrophil polarization: spatiotemporal dynamics of RhoA activity support a self-organizing mechanism. *Proc. Natl Acad. Sci. USA* **103**, 3639–3644 (2006).
17. Onsum, M. & Rao, C. V. A mathematical model for neutrophil gradient sensing and polarization. *PLoS Comput. Biol.* **3**, e36 (2007).
18. Inoue, T. & Meyer, T. Synthetic activation of endogenous PI3K and Rac identifies an AND-gate switch for cell polarization and migration. *PLoS ONE* **3**, e3068 (2008).

19. Houk, A. R. *et al.* Membrane tension maintains cell polarity by confining signals to the leading edge during neutrophil migration. *Cell* **148**, 175–188 (2012).
20. Chen, L. *et al.* Two phases of actin polymerization display different dependencies on PI(3,4,5)P3 accumulation and have unique roles during chemotaxis. *Mol. Biol. Cell* **14**, 5028–5037 (2003).
21. Gerisch, G., Malchow, D., Roos, W. & Wick, U. Oscillations of cyclic nucleotide concentrations in relation to the excitability of *Dictyostelium* cells. *J. Exp. Biol.* **81**, 33–47 (1979).
22. Gerisch, G. & Hess, B. Cyclic-AMP-controlled oscillations in suspended *Dictyostelium* cells: their relation to morphogenetic cell interactions. *Proc. Natl Acad. Sci. USA* **71**, 2118–2122 (1974).
23. Postma, M. *et al.* Uniform cAMP stimulation of *Dictyostelium* cells induces localized patches of signal transduction and pseudopodia. *Mol. Biol. Cell* **14**, 5019–5027 (2003).
24. Lappano, S. & Coukell, M. B. Evidence that intracellular cGMP is involved in regulating the extracellular cAMP phosphodiesterase and its specific inhibitor in *Dictyostelium discoideum*. *Dev. Biol.* **93**, 43–53 (1982).
25. Futrelle, R. P., Traut, J. & McKee, W. G. Cell behavior in *Dictyostelium discoideum*: preaggregation response to localized cyclic AMP pulses. *J. Cell Biol.* **92**, 807–821 (1982).
26. Meinhardt, H. Orientation of chemotactic cells and growth cones: models and mechanisms. *J. Cell. Sci.* **112**, (Pt 17): 2867–2874 (1999).
27. Xiong, Y., Huang, C. H., Iglesias, P. A. & Devreotes, P. N. Cells navigate with a local-excitation, global-inhibition-biased excitable network. *Proc. Natl Acad. Sci. USA* **107**, 17079–17086 (2010).
28. Neilson, M. P. *et al.* Chemotaxis: a feedback-based computational model robustly predicts multiple aspects of real cell behaviour. *PLoS Biol.* **9**, e1000618 (2011).
29. Nishikawa, M., Horning, M., Ueda, M. & Shibata, T. Excitable signal transduction induces both spontaneous and directional cell asymmetries in the phosphatidylinositol lipid signaling system for eukaryotic chemotaxis. *Biophys. J.* **106**, 723–734 (2014).
30. Shibata, T., Nishikawa, M., Matsuoka, S. & Ueda, M. Intracellular encoding of spatiotemporal guidance cues in a self-organizing signaling system for chemotaxis in dictyostelium cells. *Biophys. J.* **105**, 2199–2209 (2013).
31. Huang, C. H., Tang, M., Shi, C., Iglesias, P. A. & Devreotes, P. N. An excitable signal integrator couples to an idling cytoskeletal oscillator to drive cell migration. *Nat. Cell. Biol.* **15**, 1307–1316 (2013).
32. Charest, P. G. *et al.* A Ras signaling complex controls the RasC-TORC2 pathway and directed cell migration. *Dev. Cell* **18**, 737–749 (2010).
33. Kortholt, A., King, J. S., Keizer-Gunnink, I., Harwood, A. J. & Van Haastert, P. J. Phospholipase C regulation of phosphatidylinositol 3,4,5-trisphosphate-mediated chemotaxis. *Mol. Biol. Cell* **18**, 4772–4779 (2007).
34. Kortholt, A. *et al.* *Dictyostelium* chemotaxis: essential Ras activation and accessory signalling pathways for amplification. *EMBO Rep.* **12**, 1273–1279 (2011).
35. Hecht, I. *et al.* Activated membrane patches guide chemotactic cell motility. *PLoS Comput. Biol.* **7**, e1002044 (2011).
36. Cooper, R. M., Wingreen, N. S. & Cox, E. C. An excitable cortex and memory model successfully predicts new pseudopod dynamics. *PLoS ONE* **7**, e33528 (2012).
37. Bretschneider, T. *et al.* Dynamic actin patterns and Arp2/3 assembly at the substrate-attached surface of motile cells. *Curr. Biol.* **14**, 1–10 (2004).
38. Iglesias, P. A. & Shi, C. A comparison of adaptation motifs: Temporal, stochastic and spatial responses. *IET Sys. Biol* doi:

39. Ma, W., Trusina, A., El-Samad, H., Lim, W. A. & Tang, C. Defining network topologies that can achieve biochemical adaptation. *Cell* **138**, 760–773 (2009).
40. Janetopoulos, C., Jin, T. & Devreotes, P. Receptor-mediated activation of heterotrimeric G-proteins in living cells. *Science* **291**, 2408–2411 (2001).
41. Iglesias, P. A. & Devreotes, P. N. Biased excitable networks: how cells direct motion in response to gradients. *Curr. Opin. Cell Biol.* **24**, 245–253 (2012).
42. Vicker, M. G. Eukaryotic cell locomotion depends on the propagation of self-organized reaction-diffusion waves and oscillations of actin filament assembly. *Exp. Cell. Res.* **275**, 54–66 (2002).
43. Weiner, O. D., Marganski, W. A., Wu, L. F., Altschuler, S. J. & Kirschner, M. W. An actin-based wave generator organizes cell motility. *PLoS Biol.* **5**, e221 (2007).
44. Gerisch, G. *et al.* Mobile actin clusters and traveling waves in cells recovering from actin depolymerization. *Biophys. J.* **87**, 3493–3503 (2004).
45. Arai, Y. *et al.* Self-organization of the phosphatidylinositol lipids signaling system for random cell migration. *Proc. Natl Acad. Sci. USA* **107**, 12399–12404 (2010).
46. Bretschneider, T. *et al.* The three-dimensional dynamics of actin waves, a model of cytoskeletal self-organization. *Biophys. J.* **96**, 2888–2900 (2009).
47. Asano, Y., Nagasaki, A. & Uyeda, T. Q. Correlated waves of actin filaments and PIP3 in Dictyostelium cells. *Cell. Motil. Cytoskeleton* **65**, 923–934 (2008).
48. Shi, C., Huang, C. H., Devreotes, P. N. & Iglesias, P. A. Interaction of motility, directional sensing, and polarity modules recreates the behaviors of chemotaxing cells. *PLoS Comput. Biol.* **9**, e1003122 (2013).
49. Veltman, D. M., Keizer-Gunnik, I. & Van Haastert, P. J. Four key signaling pathways mediating chemotaxis in Dictyostelium discoideum. *J. Cell Biol.* **180**, 747–753 (2008).
50. Hoeller, O. & Kay, R. R. Chemotaxis in the absence of PIP3 gradients. *Curr. Biol.* **17**, 813–817 (2007).
51. Srinivasan, K. *et al.* Delineating the core regulatory elements crucial for directed cell migration by examining folic-acid-mediated responses. *J. Cell Sci.* **126**, 221–233 (2013).
52. Veltman, D. M., Lemieux, M. G., Knecht, D. A. & Insall, R. H. PIP3-dependent macropinocytosis is incompatible with chemotaxis. *J. Cell Biol.* **204**, 497–505 (2014).
53. Iijima, M. & Devreotes, P. Tumor suppressor PTEN mediates sensing of chemoattractant gradients. *Cell* **109**, 599–610 (2002).
54. Kohout, T. A. & Lefkowitz, R. J. Regulation of G protein-coupled receptor kinases and arrestins during receptor desensitization. *Mol. Pharmacol.* **63**, 9–18 (2003).
55. Hadwiger, J. A., Lee, S. & Firtel, R. A. The G alpha subunit G alpha 4 couples to pterin receptors and identifies a signaling pathway that is essential for multicellular development in Dictyostelium. *Proc. Natl Acad. Sci. USA* **91**, 10566–10570 (1994).
56. Kumagai, A., Hadwiger, J. A., Pupillo, M. & Firtel, R. A. Molecular genetic analysis of two G alpha protein subunits in Dictyostelium. *J. Biol. Chem.* **266**, 1220–1228 (1991).
57. Liao, X. H., Bugghey, J., Lee, Y. K. & Kimmel, A. R. Chemoattractant stimulation of TORC2 is regulated by receptor/G protein-targeted inhibitory mechanisms that function upstream and independently of an essential GEF/Ras activation

12/23/2014 Evolutionarily conserved coupling of adaptive and excitable networks mediates eukaryotic chemotaxis : Nature Communications : Nature Publishing Gr...
pathway in *Dictyostelium*. *Mol. Biol. Cell* **24**, 2146–2155 (2013).

58. Pitt, G. S. *et al.* Structurally distinct and stage-specific adenylyl cyclase genes play different roles in *Dictyostelium* development. *Cell* **69**, 305–315 (1992).
59. Wu, L., Valkema, R., Van Haastert, P. J. & Devreotes, P. N. The G protein beta subunit is essential for multiple responses to chemoattractants in *Dictyostelium*. *J. Cell Biol.* **129**, 1667–1675 (1995).
60. Peng, G. E., Wilson, S. R. & Weiner, O. D. A pharmacological cocktail for arresting actin dynamics in living cells. *Mol. Biol. Cell* **22**, 3986–3994 (2011).
61. Cai, H., Huang, C. H., Devreotes, P. N. & Iijima, M. Analysis of chemotaxis in dictyostelium. *Methods Mol. Biol.* **757**, 451–468 (2012).
62. Kamimura, Y. *et al.* PIP3-independent activation of TorC2 and PKB at the cell's leading edge mediates chemotaxis. *Curr. Biol.* **18**, 1034–1043 (2008).
63. Postma, M. & Van Haastert, P. J. A diffusion-translocation model for gradient sensing by chemotactic cells. *Biophys. J.* **81**, 1314–1323 (2001).

Download references

Acknowledgements

We thank A. Kortholt and P. Van Haastert (University of Groningen) for the RBD-GFP construct as well as sGC and sGC⁻/plaA⁻/piaA⁻ cells, R. Kay (MRC Laboratory of Molecular Biology, UK) for AX2 cells, G. Gerisch (Max Planck Institute for Biochemistry, Germany) for the LimE-RFP construct, M. Morimatsu and M. Ueda (Osaka University) for the Gα2-Cerulean and Gβ-Venus constructs, C. Cooper (Johns Hopkins University) for FUW lentivirus packaging system and members of the Devreotes and Iglesias labs for helpful suggestions. This work was supported in part by grants from the National Institutes of Health, GM28007 (to P.N.D.), GM34933 (to P.N.D.) and GM71920 (to P.A.I.), and a Harold L. Plotnick Fellowship from the Damon Runyon Cancer Research Foundation, DRG2019-09 (to C.H.H.).

Author information

These authors contributed equally to this work

Ming Tang & Chuan-Hsiang Huang

Affiliations

Department of Cell Biology, Johns Hopkins University School of Medicine, 725 North Wolfe Street, WBSB 116, Baltimore, Maryland 21205, USA

Ming Tang, Mingjie Wang, Pablo A. Iglesias, Peter N. Devreotes & Chuan-Hsiang Huang

Department of Physiology and Pathophysiology, Fudan University Shanghai Medical College, 138 Yi Xue Yuan Road, Shanghai 200032, China

Mingjie Wang

Department of Electrical and Computer Engineering, Johns Hopkins University, 3400 North Charles Street, 226 Barton Hall, Baltimore, Maryland 21218, USA

Changji Shi & Pablo A. Iglesias

Contributions

M.T., C.-H.H. and M.W. performed the experiments. C.S. and P.A.I. carried out computer simulations. All authors analysed the

Competing financial interests

The authors declare no competing financial interests.

Corresponding authors

Correspondence to: Peter N. Devreotes or Chuan-Hsiang Huang

Supplementary information

PDF files

1. Supplementary Information (6,468 KB)
Supplementary Figures 1-5, Supplementary Table 1 and Supplementary References

Movies

1. Supplementary Movie 1 (678 KB)
Responses to sequential stimulation by cAMP and folic acid. Time-lapse video of Dictyostelium cells expressing PH-GFP and developed in DB buffer for 1.5 hour. Global 10 μ M cAMP was added at 20 s, and a micropipette containing 100 μ M folic acid was introduced to the viewing field at 2 min for 20 s. The video was captured every 2 s and shown at 15 frames per second.
2. Supplementary Movie 2 (1,910 KB)
PH-GFP and C5aR-RFP in HL-60 cells. Time-lapse TIRF video of HL-60 neutrophils expressing PH-AKT-GFP and C5aR-RFP immobilized by JLY cocktail. The video was captured every 3 s and shown at 30 frames per second.

Nature Communications ISSN (online) 2041-1723

© 2014 Macmillan Publishers Limited. All Rights Reserved.

partner of AGORA, HINARI, OARE, INASP, ORCID, CrossRef and COUNTER